RIBAGUA – Revista Iberoamericana del Agua 3 (2016) 25–33

RIBAGUA

www.elsevier.es/ribagua

Technical article

Application of 2D numerical simulation for the analysis of the February 2014 Bolivian Amazonia flood: Application of the new HEC-RAS version 5

V. Moya Quiroga[a,b,*], S. Kure[a], K. Udo[a], A. Mano[a]

[a] International Research Institute of Disaster Science, Tohoku University, Sendai, Japan
[b] Instituto de Hidráulica e Hidrología, UMSA, La Paz, Bolivia

ARTICLE INFO

Article history:
Received 27 July 2015
Accepted 23 December 2015
Available online 13 February 2016

Keywords:
Two-dimensional simulation
Flood simulation
HEC-RAS
Flood hazard
Bolivian Amazonia

ABSTRACT

Llanos de Moxos are vast plains in the Bolivian Amazonia that are continually flooded by the Mamore river. The flood lasts for several days affecting important cities like Trinidad, drowning people, drowning cattle and swamping arable land. Because of the cloudy skies, remote sensing observations are limited to some areas and few days. Thus, there is huge uncertainty about characteristics of flood events and possible consequences. Two-dimensional (2D) numerical simulation proved to be an important tool for understanding flood events. The HEC-RAS model is one of the most popular hydraulic models. In 2014 a new version of HEC-RAS (HEC-RAS-v5) was released including 2D capabilities. The present study applied the new HEC-RAS-v5 to simulate the February 2014 flood event in the Bolivian Amazonia. The flood simulated shows good performance when compared with satellite image of the flood event. In addition, the simulation provides information like water depth, flow velocity and a temporal variation of the flood. Specific locations where water begins to overflow were identified. Over most of the flooded area the water velocity is lower than 0.25 m s^{-1}. During first ten days of the flood the flood extent increases rapidly. The flood depth allows identifying areas exposed to different hazard levels. The west plain of the Mamore river is the most exposed to the flood; it shows bigger flood extent, longer flood duration and deeper water depth. The flood that threatens the city of Trinidad originates in two locations; one located 32 km at the north and other located 10 km at the south west. The flood from the north gets close to Trinidad twelve days after it begins to overflow, while the flood from the south gets close to Trinidad seven days after it begins to overflow. Although the flood from the north is deeper than the flood from the south, the flood from the south begins flooded before the north. Thus, water borne and vector borne diseases may originate at the south earlier than the north. The city of San Javier gets covered by flood five days after the water begins to overflow. The study shows the applicability and the value of the 2D capabilities of the new HEC-RAS for flood studies.

Aplicación de simulación numérica 2D para analizar la inundación de febrero de 2014 en la Amazonia Boliviana: aplicación del nuevo HEC-RAS versión 5

Palabras clave:
Simulación bidimensional
Simulación de inundación
HEC-RAS
Amenaza de inundación
Amazonia Boliviana

RESUMEN

Llanos de Moxos son planicies de inundación en la Amazonia Boliviana que constantemente son inundadas por el río Mamore. Las inundaciones se prolongan durante varios días afectando importantes ciudades como Trinidad, ahogando gente, ahogando ganado e inundando cultivos. La visibilidad de imágenes satelitales se ve limitada debido a la nubosidad. Por tal motivo se tiene un gran desconocimiento sobre las características de la inundación y sus posibles consecuencias. Simulación numérica bidimensional (2D) es una importante herramienta para simular y analizar inundaciones. El modelo HEC-RAS es

* Corresponding author.
E-mail addresses: vladyman@hotmail.co.uk, moyav@potential1.civil.tohoku.ac.jp (V. Moya Quiroga).

http://dx.doi.org/10.1016/j.riba.2015.12.001

uno de los más populares modelos hidráulicos. En octubre de 2014 la última versión de HEC-RAS versión 5 fue publicada con capacidades 2D. El presente estudio aplicó el nuevo HEC-RAS versión 5 para simular la inundación de febrero de 2014 en la Amazonia Boliviana. La inundación simulada muestra buen desempeño comparado con imagen satelital del evento. Además, la simulación provee información adicional como puede ser profundidad de agua, velocidad del flujo y la variación de la inundación en el tiempo. Se identificaron lugares específicos donde el agua comienza a inundar la planicie. En la mayor parte del área inundada la velocidad del flujo es inferior a 0,25 m s^{-1}. Durante los primeros diez días de inundación la extensión de la inundación se incrementa rápidamente. La profundidad de la inundación permite identificar zonas expuestas a distintos niveles de amenaza. La planicie al oeste del río Mamore es la más expuesta a la inundación; esta tiene mayor área inundada, duración más prolongada y mayor profundidad de inundación. La inundación que amenaza a Trinidad se origina en dos lugares; uno ubicado unos 32 km al norte de Trinidad y el otro ubicado unos 10 km al sudoeste. La inundación del norte se acerca a Trinidad en unos doce días después de iniciarse la inundación, mientras que la inundación del sudoeste se acerca a Trinidad unos siete días después de iniciarse la inundación. Pese a que la inundación del norte muestra mayor profundidad de inundación, la inundación del sur llega a Trinidad antes. Por tal motivo, es posible que brotes de enfermedades se originen en el sur. La ciudad de San Javier queda inundada unos cinco días después de iniciarse la inundación. El presente estudio muestra la aplicabilidad y los posibles beneficios de las nuevas capacidad 2D del nuevo HEC-RAS para estudio de inundaciones.

1. Introduction

Floods can be considered as the most important natural disaster with an occurrence higher than any other natural hazard and affecting more people than all the other natural hazards together [1]. Besides, climate change will increase flood probabilities and the magnitude of floods [2]. Floods are related to social–civil conflicts [3], environmental problems [4] and economic losses [5]. The Llanos de Moxos located in the Bolivian Amazonia are an example of floodplains that continually suffer severe flood events causing environmental, economic and social damages. Several hectares of arable land get swamped, several thousands of cattle heads are drowned, crops are flooded and some important cities are either flooded or threatened by flood waters. Besides, due to the flat topographic characteristics of the area the floods last for several days; hence, people are also exposed to water borne and vector borne diseases. Flood risk management measures are required for the Llanos de Moxos.

Flood risk assessment and management are fundamental steps for identifying current hazards, prone risk areas and reducing them in future flood events [6]. In order to propose flood management measures it is important to understand the flood and to analyze the effect of the proposed measures. A simple approach is to analyze floods based on in situ flood observations [7]. However, in situ flood observations are not always available. Other studies use remote sensing data for flood studies [8,9]. However, usually flood events occur during cloudy skies that limit the use of remote sensing data. Besides, flood studies based on observation are only valid for specific flood events. Hence, future flood events or the effect of flood structural measures cannot be analyzed by such observation based maps. The use of numerical models allows simulating flood events considering different scenarios. Hence, numerical models are important tools for understanding flood events, flood hazard assessment and flood management planning. Previous studies showed the applicability of numerical models for producing hazard maps considering different flood management strategies [10,11] or reconstructing past flood events [12].

Numerical models may use either one-dimensional (1D) or two-dimensional (2D) models. Although the 1D modelling approach could be useful in some contexts, mainly for artificial channels, it presents several limitations for overflow analysis [13]. When water begins to overflow it becomes a 2D phenomenon and the use of a 2D model is more suitable. Thus, 2D numerical models were successfully applied for flood modelling [14–16]; the discharge is used as upstream boundary condition of the main river channel and then a 2D simulation is performed. Nowadays there is a wide availability of numerical models with different capabilities and from different developers; some models are free while others require the purchase of a licence. One of the most popular hydraulic models is the American model HEC-RAS developed by the U.S. Army Corps of Engineers (USACE). HEC-RAS is a free software with a friendly graphical user interface that was successfully used for flood studies [17–19]. Moreover, it is under constant improvement and development by the USACE. However, one of its greatest limitations was that it was limited to 1D flows. Thus, studies usually combined HEC-RAS with other models 2D; flow discharges at certain cross section are used as boundary condition for the 2D model [16]. Last year (2014) HEC-RAS announced and released its new HEC-RAS version 5.0 Beta (HEC-RAS-v5) with 2D capabilities [20]. The model is still distributed as beta version and not fully available. Due to the popularity of HEC-RAS, this new 2D capabilities are a great innovation for future flood studies.

The present study aims to analyze the 2014 flood event in Llanos de Moxos using the 2D capabilities of the new HEC-RAS-v5. A 2D numerical simulation of the 2014 Llanos de Moxos flood event was performed with the new HEC-RAS-v5 and daily discharges of the Mamore river. The model provided daily simulation of the flood extent, flood depth and flow velocities. The simulated flood extent shows good performance when comparing to the flood extent observed by satellite image.

2. Study area and data

2.1. Study area

Llanos de Moxos are vast floodplains between latitudes 12.0° S and 17.0° S and longitudes 62.5° W and 67.0° W in the Bolivian Amazonia. They have a mean elevation below 150 m above sea level and a gentle slope lower than 10 cm km^{-1}. The central part of Llanos de Moxos is a floodplain subject to severe inundations that may inundate up to 150 000 km^2 affecting thousands of people and lead to human-economic losses equivalent to millions of U.S. dollars [21]. The low gradient and the impermeable clayey soils favour the inundation [22]. The main river is the Mamore river which is also the longest and most important Bolivian river. During the wet season the Mamore river overflows and floods the area. The most important economic activity within the study area is cattle with a production that accounts for about 42% of the Bolivian cattle. Besides cattle, crops like yucca, rice, banana and corn are also

important economic activities. This study area is also habitat of several endangered and unique animals like the pink dolphin and more than 86 fish species [23]. From a social perspective some Bolivian cities like Trinidad (14.83° W, 64.90° W) and San Javier (14.60° W, 64.88° W) are located within this region. Trinidad has more than 100 000 habitants and is the most important city in the Bolivian Amazonia.

The flood event of February 2014 was among the most severe ones. Between February 02 and February 22 the estimated discharge increased from 4 200 $m^3 s^{-1}$ to more than 13 400 $m^3 s^{-1}$ [24]. The event was so severe that it led to international discussions with Brazil about the role of the Jirau dam and special studies had to be carried out in order to analyze the possible influence of the Jirau dam [25] and the climatological conditions that led to such event [26]. The National Aeronautics and Space Administration (NASA) dedicated a web site for this flood event [27]. The Bolivian government reported that more than 69 000 families were affected, more than 40 000 ha of crops were swamped and more than 108 000 heads of cattle were drowned.

2.2. Data

The main types of data are geographic data that provides a physical description of the area and flow data that provides information about the discharge of the Mamore river. The geographic data was based on the digital elevation model (DEM) from the Shuttle radar topography mission (SRTM) with a grid cell size of 90 m. The study focused on an area located between 14.26° S, 65.24° W and 14.99° S, 64.62° W. Such area was selected because it includes the city of Trinidad which is the most important city in the Bolivian Amazonia and the location where river discharge was estimated (Los Puentes station). The flow data was based on daily discharge data of the Mamore river at Los Puentes station provided by the Flood Observatory [24]. The Flood Observatory data base contains more than 16 years of daily discharge from the Mamore river. The study simulated the floods between February 02, 2014 and March 02, 2014. This period was selected because it was the most effected by the flood event. Fig. 1 shows the study area and the discharge at Los Puentes. It is important to note that Los Puentes is located at the upstream extreme of the studied reach of the Mamore river.

3. Methodology

3.1. Numerical simulation

The flood event was simulated using the new HEC-RAS-v5 model developed by the USACE. The new HEC-RAS-v5 solves either the full 2D Saint Venant equations or the 2D diffusive wave equations:

$$\frac{\partial \zeta}{\partial t} + \frac{\partial p}{\partial x} + \frac{\partial q}{\partial y} = 0 \tag{1}$$

$$\frac{\partial p}{\partial t} + \frac{\partial}{\partial x}\left(\frac{p^2}{h}\right) + \frac{\partial}{\partial y}\left(\frac{pq}{h}\right) = -\frac{n^2 p g\sqrt{p^2+q^2}}{h^2} - gh\frac{\partial \zeta}{\partial x} + pf + \frac{\partial}{\rho \partial x}(h\tau_{xx}) + \frac{\partial}{\rho \partial y}(h\tau_{xy}) \tag{2}$$

$$\frac{\partial q}{\partial t} + \frac{\partial}{\partial y}\left(\frac{q^2}{h}\right) + \frac{\partial}{\partial x}\left(\frac{pq}{h}\right) = -\frac{n^2 q g\sqrt{p^2+q^2}}{h^2} - gh\frac{\partial \zeta}{\partial y} + qf + \frac{\partial}{\rho \partial y}(h\tau_{yy}) + \frac{\partial}{\rho \partial x}(h\tau_{xy}) \tag{3}$$

where h is the water depth (m), p and q are the specific flow in the x and y directions ($m^2 s^{-1}$), ζ is the surface elevation (m), g is the acceleration due to gravity ($m s^{-2}$), n is the Manning resistance, ρ is the water density ($kg m^{-3}$), τ_{xx}, τ_{yy} and τ_{xy} are the components of the effective shear stress and f is the Coriolis (s^{-1}). When the diffusive wave is selected the inertial terms of the momentum equations (Eqs. (2) and (3)) are neglected.

Initially, the present study considered both options the full Saint Venant equations and the 2D diffusive wave. Both methods provided the same results, but simulation solving the 2D diffusive wave equations was about 20 times faster. Thus, the 2D diffusive wave equations were used for the analysis. The computing domain is defined by a closed polygon and the computation cells are created inside the polygon. The computation cells may be arranged in a staggered or a non-staggered grid composed by polygons between 3 sides and 8 sides. The present study used a staggered grid composed by rectangular cells 90 m by 90 m. Such grid was selected in order to stay close to the original DEM (SRTM 90*90). The selected equations are solved with an implicit finite volume algorithm. The finite volume solution approximates the average integral on a reference volume and allows a more general approach to unstructured meshes. The solution of the equations is similar to the HEC-RAS 1D unsteady flow solution. Hydraulic property tables are computed before starting calculations. Elevation–volume relationships are computed for each cell and elevation–hydraulic properties (wetted perimeter, area) relationships are computed for every computational cell face, similar to the cross section pre-processing in 1D. Then, the equations are solved with an iterative scheme with a maximum of 40 iterations.

HEC-RAS-v5 can be used either as a fully 2D model or as a hybrid 1D2D model when the main rivers are modelled as 1D and the floodplains are modelled as 2D. Although a hybrid 1D2D model tends to be faster than a 2D model, such 1D2D model requires the user to define the connections between the 1D and the 2D models. Such connections require a prior definition of the overflow locations. The present study used a full 2D model because the overflow locations were unknown. Future research may use the present results in order to perform a 1D2D model considering the defined overflow locations.

The present study used two types of boundary conditions: one hydrograph boundary condition and one normal depth boundary condition. The hydrograph boundary condition was located at the upstream extreme of the Mamore river (at Los Puentes station) representing the observed discharge that enters the Mamore river and the simulation domain. The 450 m width of the Mamore river were represented by four cells. The inflow hydrograph (Fig. 2) was defined at these four cells. Besides the flow hydrograph, it is important to define an energy slope that is used for distributing the discharge over the cells that integrate the boundary; the distribution is based on the specified slope and the pre-processed hydraulic properties of each cell. Considering the conditions of the study area a slope of 0.0001 $m m^{-1}$ was used. The normal depth boundary condition was located not only at the downstream extreme of the Mamore river but also at the borders of the model where the water is supposed to flow. If the border of the model is defined as a closed boundary, the model will assume that water that reaches the border reaches an obstacle. Thus, the flood water at the border will either accumulate or change direction. On the other hand, when the borders are assumed as open boundary the model assumes that the flood water that reaches the border will continue flowing outside the model domain.

In order to ensure the stability of the model, the time step was estimated according to the Courant–Friedrichs–Lewy condition:

$$Cr = \frac{c\Delta t}{\Delta x} = \frac{\sqrt{gh}\Delta t}{\Delta x} \leq 1 \tag{4}$$

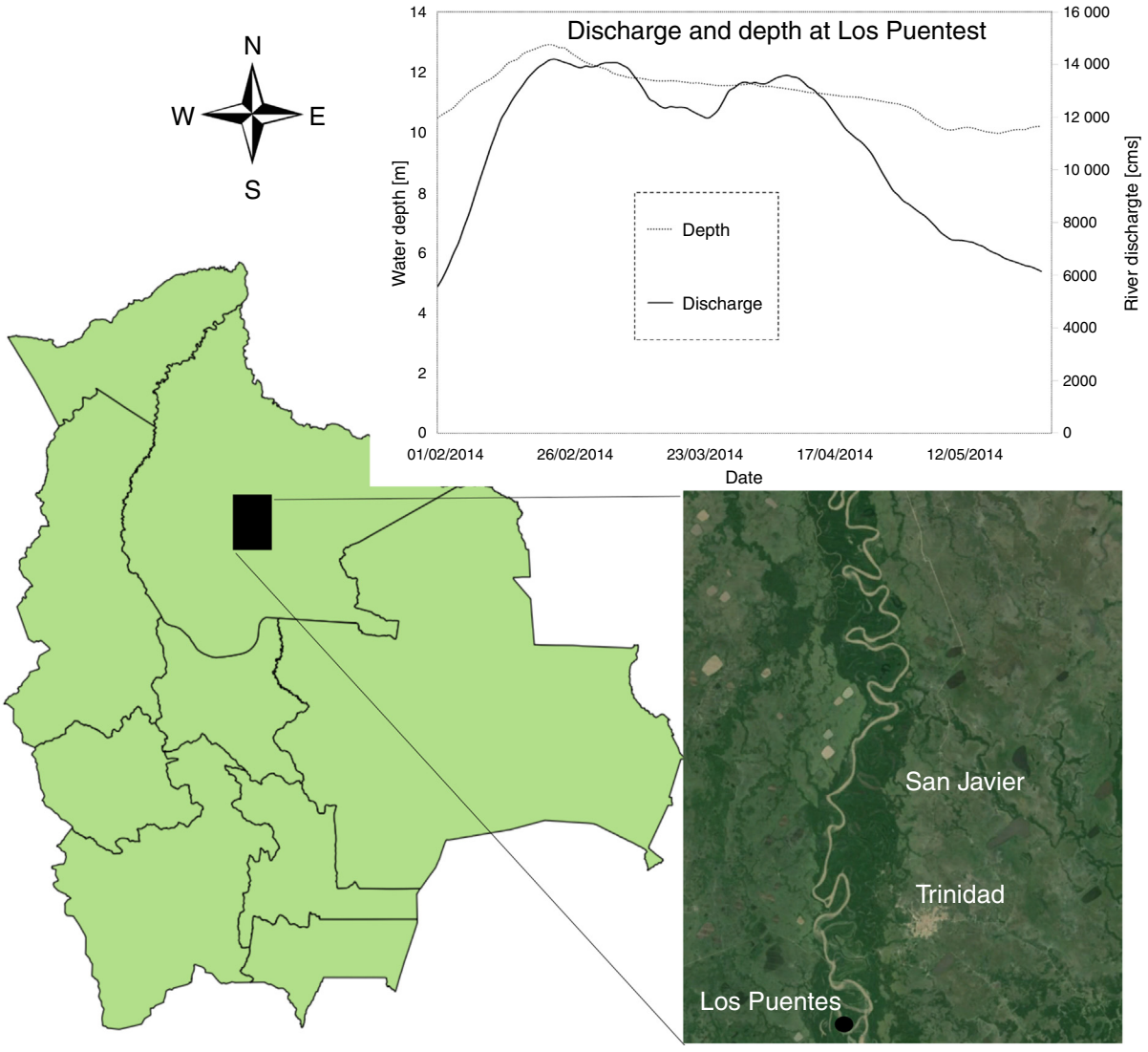

Fig. 1. Study area and discharge of the Mamore river at Los Puentes between February 02, 2014 and March 02, 2014.

where Cr is the Courant number, g is the gravity acceleration ($m\,s^{-2}$), c is the celerity ($m\ s^{-1}$) h is the flow depth (m), Δt is the time step (s) and Δx is the grid cell size (m). The celerity was estimated considering that the limnimetric station at Los Puentes reported a maximum water depth about 13 m [28]. Thus, according to Eq. (4) a time step of 15 s was selected. The roughness resistance was estimated based on the suggestions by Chow et al. [29] and a previous study that analyzed different roughness values for the study area [30]. The roughness coefficient was selected based on a sensitivity analysis. Table 1 summarizes the data used. The study simulated the flood event considering the discharge measured at Los Puentes as the upstream boundary condition. The station Los Puentes is located at the upstream extreme of the Mamore river in the study area.

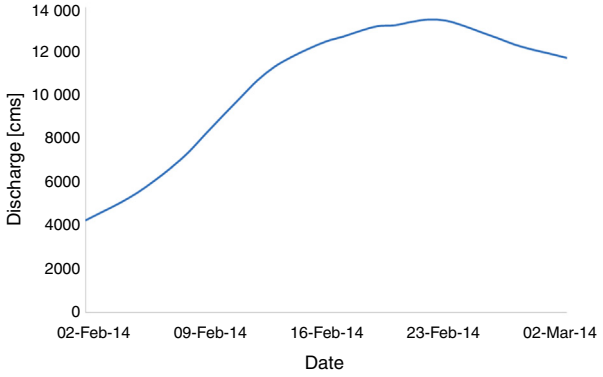

Fig. 2. Input hydrograph used in the present study.

3.2. Simulation performance

The flood simulation was compared with the flood image observed on February 17 by the Terra Aqua satellite. The

Table 1
Data used. Δt is the time step, Δx is the grid cell size, n is the Manning roughness.

Data	Value
Δt [s]	15
Δx [m]	90
n (river)	0.018–0.022
n (floodplain)	0.025–0.031
Hydrograph	Obtained from [24]
Simulation period	February 02, 2014–March 02, 2014

Table 2
flood hazard classification according to [33].

Flood hazard	Depth [m]	Hazard
H1	<0.50	Very low
H2	0.50–1.0	Low
H3	1.0–2.0	Medium
H4	2.0–5.0	High
H5	>5.0	Extreme

performance of the model was evaluated based on the measure of fit *F1* and *F2* [31] [32].

$$F1 = \frac{A}{A+B+C} \quad (5)$$

$$F2 = \frac{A-B}{A+B+C} \quad (6)$$

where *A* is the flood area correctly predicted by the model, *B* is the over predicted flood area (observed dry cells simulated as flooded cells) and *C* is the under predicted flood area (observed flooded cells simulated as dry cells by the model). The value of *F1* ranges from 0 to +1 and *F2* ranges from −1 to +1. Values closer to +1 means a better performance. Then, flood hazard to people was analyzed according the results from the model. The flood water depths were classified into flood hazard categories to prevent human damage according to the Japanese criteria of the Ministry of Land Infrastructure and Transport (MLIT) [33]. The criteria suggest the classification of five flood hazard categories (Table 2). Flood hazard H1 (flood depth lower than 0.5 m) or very low hazard means that the flood does not pose hazard to people and on foot evacuation is not difficult. Flood hazard H2 (flood depth between 0.5 m and 1.0 m) or low hazard means that flood water poses hazard for infants and on foot evacuation of adults becomes difficult; evacuation becomes more complicated. Flood hazard H3 (flood depth between 1.0 m and 2.0 m) is medium hazard; although flood depth can drown people, people may be safe inside their homes. Flood hazard H4 (flood depth between 2.0 m and 5.0 m) or high hazard means that people are exposed to hazard even inside their homes and are suggested to evacuate towards the roof of their homes. Flood hazard H5 or extreme hazard means that even man-made structures like homes may get covered by the flood; people may get drowned even if they evacuate towards the roof of their homes.

4. Results and discussion

4.1. Performance

This version of HEC-RAS uses double-precision floating point numbers for elevations when storing data to internal memory. However, when the data is written to a results file HEC-RAS version stores the results with a precision of six digits (five numbers and a decimal point). Since the highest water depths were deeper than 10 m (2 digits), the simulations results had a precision of 1 mm. The performance of the model was assessed by comparing the flood simulation with a remotely sensed image from the flood event. The performance assessment considered the flood registered by the moderate resolution imaging spectroradiometer (MODIS) aboard the Aqua satellite on February 17, 2014. The specific day was selected because it is the only image of the area during the flood event with clear skies. Fig. 3 shows the flood registered by MODIS on February 17, 2014 and the flood simulated by the new HEC-RAS version 5. The model provides a good agreement with the observed flood. Table 3 summarizes the performance of the model considering different roughness values. In all the cases the model evaluation provides measure of fit values *F1* and *F2* higher than 0.6. Such values are higher than values accepted by other studies [31,32,34]; this shows that the model successfully reproduces the flood event. The values *F1* and *F2* are very similar for all the scenarios despite the different roughness values. This shows that the sensitivity of the roughness value within the proper range is small compared with the scale of the flood event. Although all the roughness values considered provide acceptable results, the present study considered only the roughness value with the best performance (option 1).

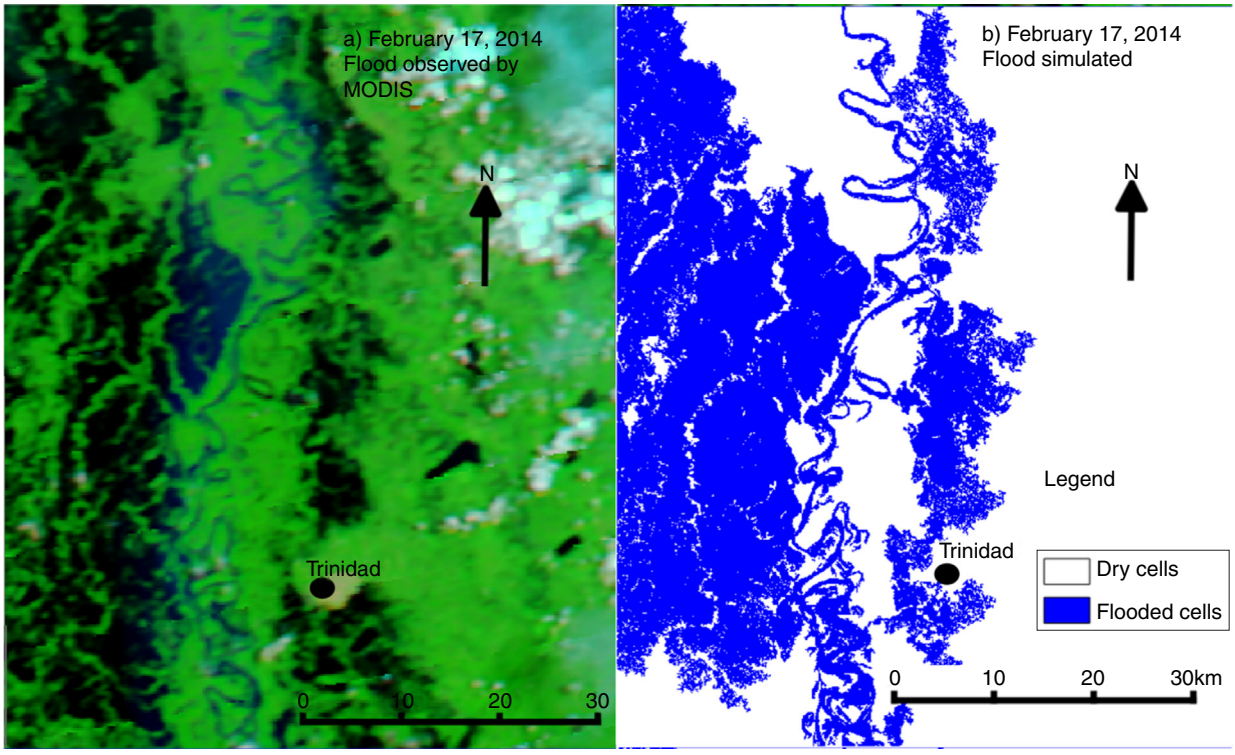

Fig. 3. Flood extent of February 17, 2014 registered by MODIS and flood extent on February 17, 2014 simulated by the HEC-RAS model.

Table 3
Performance of the model with different roughness coefficients for the channel (c) and the floodplain (fp). FS is the simulated flood extent, FO is the observed flood extent, *A* is the number of correctly flood simulated cells, *B* is the number of over-predicted flood cells, *C* is the number of under-predicted flood cells, *F1* and *F2* are measure of fit.

Roughness	FS [km^2]	FO [km^2]	FO/FS	A	B	C	*F1*	*F2*
0.020 (c) 0.031 (fp)	2016	2330	0.87	486 380	53 869	125 479	0.73	0.65
0.022 (c) 0.035 (fp)	2010	2330	0.86	485 462	54 207	126 059	0.72	0.65
0.018 (c) 0.025 (fp)	1905	2330	0.82	481 209	50 679	133 840	0.72	0.65

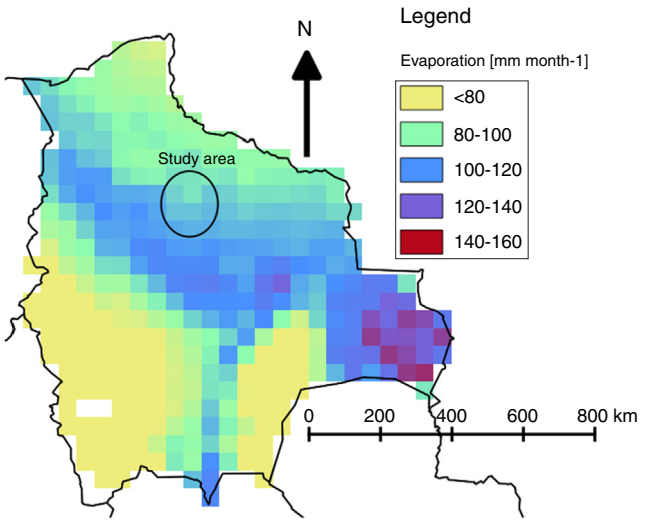

Fig. 4. Potential evaporation of Bolivia during February 2014 obtained from [35]. The circle shows the study area.

The main limitation of the model is that its simulated extent covers about 13% less area than the flood from the remotely sensed image. This difference may be explained by two causes: (a) the model only considered the Mamore river and not the other rivers. Thus, discharge overflow from minor rivers blocked by the Mamore river is not considered by the model. (b) Some observed flood cells may be caused by endogenic processes; once the ground is saturated any additional precipitation gets ponded. Table 3 summarizes the performance of the model. Although the model does not consider some hydrological processes like infiltration or evaporation that could reduce the flood volume, those processes may be assumed as negligible for the purpose of the present study. Due to the low permeability of the soil [22] it is reasonable to assume that infiltration during this period is negligible. Fig. 4 shows the potential evaporation of Bolivia during February 2014 reported by the MODIS global evapotranspiration project [35]. The monthly evaporation during February 2014 in the study area was about 100 mm. Although the evaporation in the study area is among the highest evaporation rates of Bolivia, the evaporation may be assumed as negligible comparted with the mean flood depth of 3.36 m. The total evaporation during February 2014 accounts for about 2.9% of the mean flood depth. Thus, it is reasonable to assume that hydrological processes of infiltration and evaporation may be assumed as negligible.

4.2. The February 2014 flood event

Fig. 5a shows the daily evolution of the flooded area and the flood volume. Fig. 5b shows the relation between flood volume and flood extent. Until February 12 both curves show the same trend increasing rapidly. Then, the flood extent stabilizes before flood volume. This is because by February 12 flood extent already reached 78% of the total flood extent while flood volume is about 74% of the maximum flood volume. The flood volume still increases at the same rate about two more days until it reaches 80% of the maximum flood volume. The maximum simulated flood extent is registered on February 25; then the flood volume begins to decrease. This is because flood waters continue to move towards cells located outside the study area. Thus, February 25 could be assumed as the most flooded day for the study area. Fig. 5 shows that flood extent and flood volume show a good linear regression; they are related by the equation

$$Vol = 3 * 10^6 Ext - 3 * 10^8 \quad (7)$$

where *Vol* is the flood volume [m^3] and *Ext* is the flood extent [km^2]. This equation may become useful for future flood volume estimations based on remote sensing data.

Fig. 6 shows the evolution in time of the area exposed to different flood hazard categories. The flood hazard categories H1 and H2 are nearly constant during the flood event. The trend of flood hazards H3, H4 and H5 are the most important for planning evacuation strategies because at such flood categories evacuation actions are difficult or not possible. Flood hazard category 4 (H4) is the predominant flood hazard category. Between February 02 and February 12 the area exposed to different flood hazards increases rapidly; then it remains almost constant. Area exposed to flood categories H3 and H5 also remains almost constant after February 12. This shows that

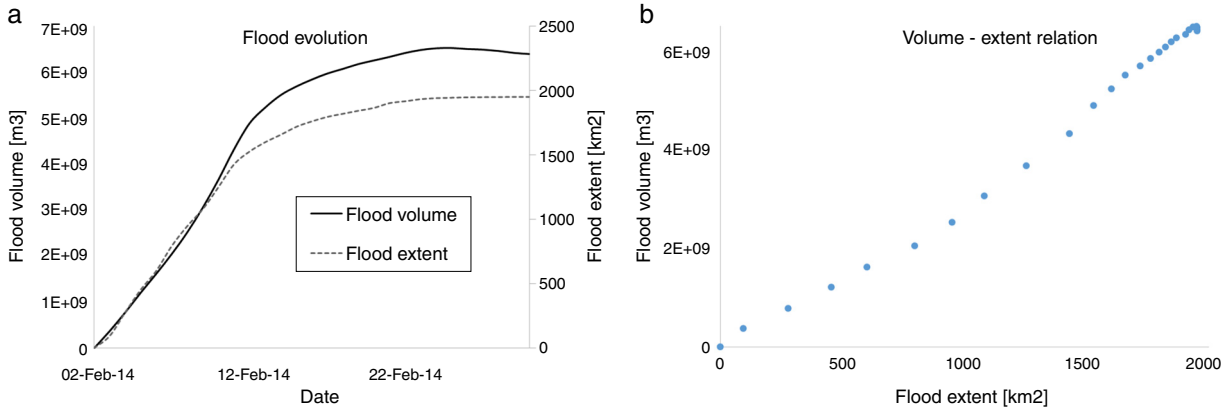

Fig. 5. Daily evolution of the flood extent and the flood volume (a) and relationship between the flood extent and the flood volume (b).

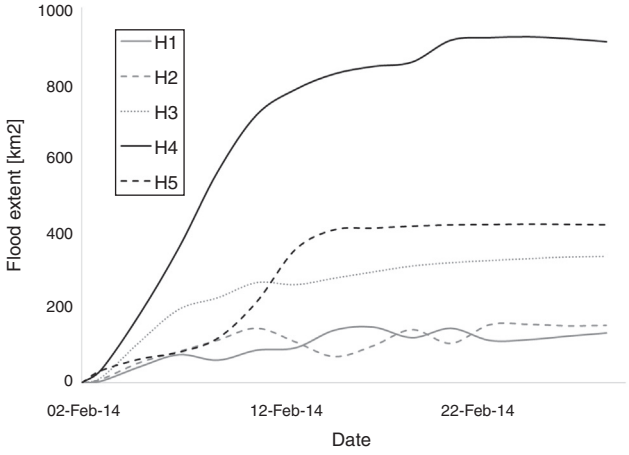

Fig. 6. Daily evolution of the flood extent exposed to different flood categories.

the first ten days of the flood can be considered as the most critical ones for evacuation. The first ten days the area exposed to flood hazard category H4 increases at a rate of 78.16 $km^2\ day^{-1}$. After February 12 the flood area exposed to flood hazard H4 increases at a rate of 11.69 $km^2\ day^{-1}$. February 25 could be considered as the most hazardous day because it shows the biggest flood extent exposed to flood hazard categories H4 and H5.

Fig. 7 shows the flow velocity on February 25. In most of the flooded areas the flood water velocity is lower than 0.25 $m\ s^{-1}$; the water is almost ponded. Such low velocities pose no hazard for people stability. Although there are no measurements of the flow velocities, the simulated velocities are reasonable when compared with the local reports and news from the events; people and cattle were standing or walking on calm waters and slow waters. This confirms that the flood hazard based only on the water depth is appropriate. The low velocities would produce low numbers of the depth velocity product. However, for the first kilometre flooded after the point A overflows the flood water has velocities about 1 $m\ s^{-1}$; velocities similar in magnitude to the river flow velocity of the Mamore river. Such high velocities show that more water overflows from this point than from the other overflow points. Besides, the areas with flood waters velocities about 1 $m\ s^{-1}$ or higher may pose additional hazard and evacuation is more difficult.

Fig. 8 shows the flood hazard map of the study area. Most of the extreme flood hazard cells (H5) are located in the rectangular lakes. The flood hazard surrounding Trinidad depends on the location. The west side has flood hazard categories H3 and H4, while the south and the north have flood hazard categories H1 and H2. Thus, evacuation measures can be achieved anywhere except the west of Trinidad. The simulated results are coincident with the reported flood depths and aerial photographs that show the city of Trinidad surrounded by water and some locations of Trinidad where flood reached depths below the waist [36]. The situation in San Javier is more critical. Not only does the flood water covers the city of San Javier but also the flood hazard is classified as H3 and H4. The simulated flood conditions in San Javier are coincident with observed flood conditions that isolated San Javier and canoes were the only mean of transportation [37]. The plains at the west margin of the Mamore not only show the biggest flood extent but also more hazardous classification; almost the whole west floodplain flood is categorized as H4. Although there are no cities located on the plains of the west margin, such plains are used for cattle. Thus, cattle located on the west margin of the Mamore river are likely to get drowned unless they are evacuated to dry land out of the flood area or to some elevated areas. Such results are coincident with aerial observations of the flood where the whole area is flooded and cattle is gathered in elevated areas that look like islands [36]. Initially, it seems that the best evacuation route for San Javier is to move 9 km to the east in order to reach safe dryland. However,

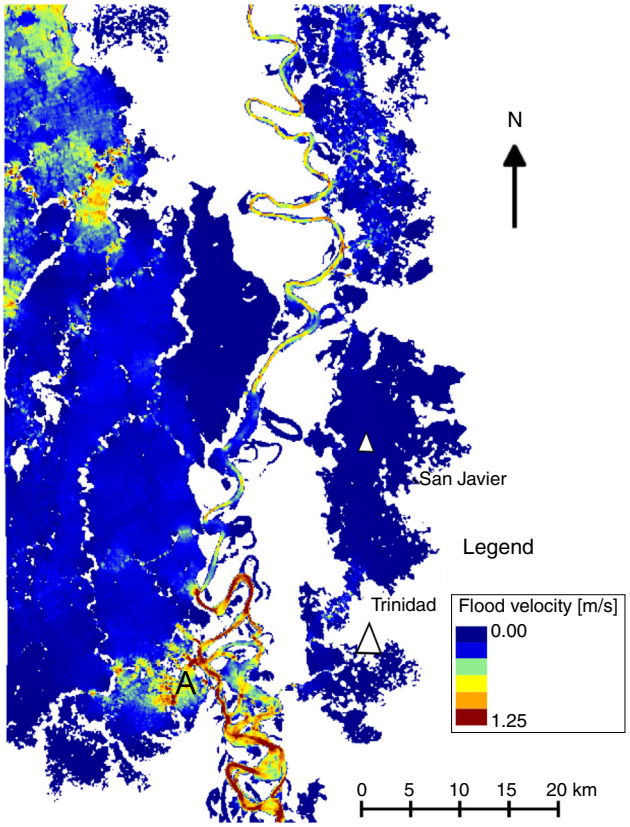

Fig. 7. Flow velocity on February 25, 2014 simulated by HEC-RAS.

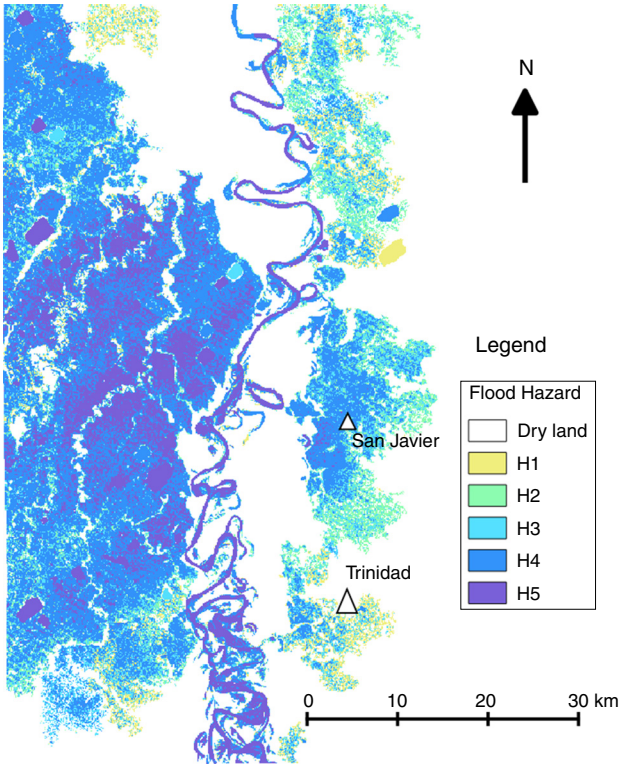

Fig. 8. Flood hazard map considering flood classification criteria from [32].

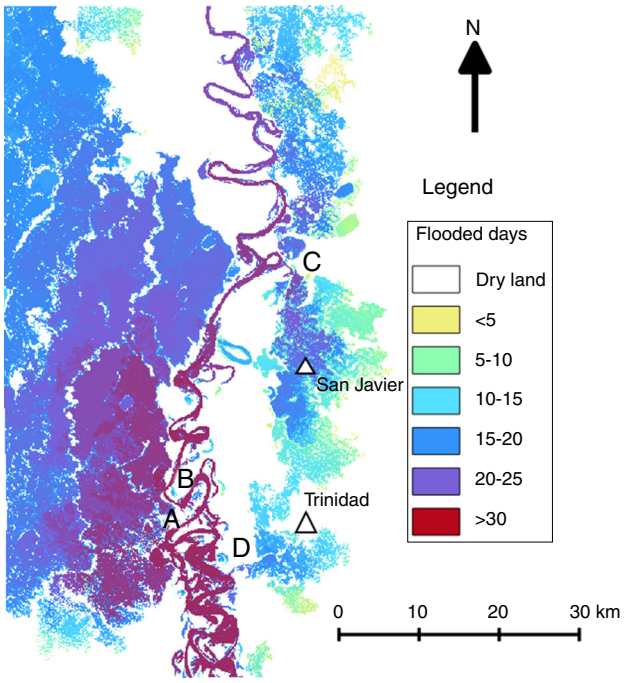

Fig. 9. Flood duration map.

that location is dryland without services. On the other hand, moving towards the south will lead to Trinidad, a bigger city with more services and hospitals. Although the distance for reaching safe dry land at the south of San Javier is about 14 km, only the first 9 km are flood waters categorized as H4. Thus, moving 9 km towards the south (same distance as when evacuating towards the east) flood waters pose little hazard. The floods that threaten the cities of San Javier and Trinidad originate at specific points where the Mamore meander is located close to the border of the meandering belt. Thus, future protection measures could analyze the possibility of including protection at these locations in order to deviate the floodwater towards other areas.

Fig. 9 shows the flood duration map. This figure also allows understanding the flood propagation; the cells with the longest flood duration are also first ones to get flooded. The flood begins at points A and B. Points A and B are points where the meander of the Mamore river is at the edge of the floodplain. The flood on the left margin of the Mamore river propagates in a north west direction. The most important overflow points on the east margin of the Mamore river are points C and D. Point C is 32 km North of Trinidad while point D is located 10 km south west of Trinidad. The overflow pattern on the east margin is different than the flood pattern of the west margin. Although point D is located upstream of point C, points C is the first to overflow. The flood from point C propagates in direction north–south. This is a direction contrary to the direction of the Mamore river. The flood that overflows from point C reaches the city of San Javier in less than five days and the North edge of Trinidad in about twelve days. The water that overflows from point D reaches the south edge of Trinidad in about seven days. It is important to note that although the flood water does not reach the city of Trinidad, the flood water surrounding Trinidad lasts for more than ten days. This flood duration is longer than the incubation period of the vector borne disease agents [38]. Besides, considering that mosquitoes may flight more than 3.5 km [39], it may be assumed that the city of Trinidad is also exposed to vector borne diseases. Such assumption is supported by official reports of dengue and malaria epidemics during flood events [40]. Moreover, considering that mosquitoes may deposit their eggs as far as 800 m from their initial location [41], dengue and malaria hatcheries could be located within the city of Trinidad. Although the flood at the south of Trinidad poses less hazard than the flood at the north of Trinidad (flood at the south is flood category H1 and flood at the North is flood category H2), the south of Trinidad gets flooded before the north of Trinidad and the flood has longer duration. Thus, water borne and vector borne diseases are expected to originate at the south of Trinidad. The flood duration map is also important for the preparedness time of San Javier and Trinidad (the time between the moment when the flood begins overflowing the Mamore river and arrives at certain location). The flood reaches San Javier in five days and Trinidad in twelve days. The flood from point D reaches Trinidad in seven days. It is important to note that the flood from point C has faster propagation than the flood from point D. Between point C and San Javier the flood propagation speed is about 2.14 km day^{-1} and from San Javier to Trinidad the propagation is about 1.9 km day^{-1}. On the other hand, the flood from point D propagates at 0.9 km day^{-1}.

5. Conclusions

The February 2014 flood event of the Llanos de Moxos was simulated using the 2D capabilities of the new HEC-RAS 5 beta.

The simulation shows good performance when comparing the simulation results with flood extent registered by satellite images. Besides, the simulation provides additional information like flood depth, flow velocity and flood duration.

The study shows that the west margin of the Mamore river is the most hazardous one; it has bigger flood extent, it has deeper flood depths and longer flood duration. On the flooded areas the water has a velocity lower than 0.25 m s^{-1}.

On the east plain of the Mamore river (where the cities of Trinidad and San Javier are located) two locations where identified as the locations where the Mamore river overflows and floods the plain. The first is located 32 km north Trinidad and the other is located 10 km south west of Trinidad.

The first ten days after the Mamore begins to overflow the flood extent increases rapidly. Thus, those ten days may be considered as the most critical ones for evacuation.

The city of San Javier is flooded five days after the Mamore river begins to overflow. The north of Trinidad is flooded twelve days after the Mamore begins to overflow and the south of Trinidad is flooded seven days after the Mamore begins to overflow.

The flood depth in Trinidad is categorized as medium hazard and low hazard and people may be safe inside their homes. On the other side, the flood depth in San Javier is categorized as high hazard and people should get on the roof of their homes in order to stay safe. The north of Trinidad shows deeper flood depth and higher hazard that could make evacuation difficult. Thus, the south of Trinidad may be an easier route of evacuation. Besides, the flood duration shows that vector borne diseases are expected to occur especially in the south of Trinidad.

The study shows that the new HEC-RAS version 5 is an important tool for studying and understanding flood events. Future applications of the new HEC-RAS version 5 may help to analyze possible flood management strategies.

Acknowledgements

The authors would like to thank the Japan Society for the Promotion of Science (JSPS). This research is financed by JSPS.

Appendix A. Supplementary data

Supplementary data associated with this article can be found, in the online version, at doi:10.1016/j.riba.2015.12.001.

References

[1] Asia Disaster Reduction Center (ARDC). Natural disaster data book 2009 (an analytical review), Kobe, Japan; 2009. p. 23.

[2] Das T, Maurer EP, Pierce DW, Dettinger MD, Cayan DR. Increases in flood magnitudes in California under warming climates. J Hydrol 2013;501:101–10, http://dx.doi.org/10.1016/j.jhydrol.2013.07.042.

[3] Ghimire R, Ferreira S, Dorfman JH. Flood-induced displacement and civil conflict. World Dev 2015;66:614–28, http://dx.doi.org/10.1016/j.worlddev.2014.09.021.

[4] Li J, Shi W. Effects of alpine swamp wetland change on rainfall season runoff and flood characteristics in the headwater area of the Yangtze River. Catena 2015;127:116–23, http://dx.doi.org/10.1016/j.catena.2014.12.020.

[5] Aerts JCJH, Botzen WJW. Climate change impacts on pricing long-term flood insurance: a comprehensive study for the Netherlands. Global Environ Change 2011;21(3):1045–60, http://dx.doi.org/10.1016/j.gloenvcha.2011.04.005.

[6] Ranzi R. Critical review of non-structural measures for water-related risks. In: Kulturisk. Delft, The Netherlands: UNESCO-IHE; 2011. p. 42.

[7] Hagen E, Lu X. Let us create flood hazard maps for developing countries. Nat Hazards 2011;58:841–3.

[8] Haq M, Akhtar M, Muhammad S, Paras S, Rahmatullah J. Techniques of remote sensing and gis for flood monitoring and damage assessment: a case study of Sindh province, Pakistan. Egypt J Rem Sens Space Sci 2012;15(2):135–41, http://dx.doi.org/10.1016/j.ejrs.2012.07.002.

[9] Chormanski J, Okruszko T, Ignar S, Batelaan O, Rebel KT, Wassen MJ. Flood mapping with remote sensing and hydrochemistry: a new method to distinguish the origin of flood water during floods. Ecol Eng 2011;37(9):1334–49, http://dx.doi.org/10.1016/j.ecoleng.2011.03.016.

[10] Di Baldassarre G, Schumann G, Bates PD. A technique for the calibration of hydraulic models using uncertain satellite observations of flood extent. J Hydrol 2009;367(3–4):276–82, http://dx.doi.org/10.1016/j.jhydrol.2009.01.020.

[11] Schober B, Hauer C, Habersak H. A novel assessment of the role of Danube floodplains in flood hazard reduction (FEM method). Nat Hazards 2015;75:33–50.

[12] Ruiz-Bellet J, Balasch J, Tuset J, Barriendos M, Mazon J, Pino D. Historical, hydraulic, hydrological and meteorological reconstruction of 1874 Santa Tecla flash floods in Catalonia (NE Iberian Peninsula). J Hydrol 2015;524:279–95.

[13] Srinivas K, Werner M, Wright N. Comparing forecast skill of inundation models of differing complexity – the case of Upton upon Severn. In: Allsop W, Samuels P, Harrop J, Huntington S, editors. Flood risk management: research and practice. London: Taylor and Francis Group; 2009., ISBN 978-0-415-48507-4.

[14] Pathirana A, Tsegaye S, Gersonius B, Vairavamoorthy K. A simple 2-D inundation model for incorporating flood damage in urban drainage planning. Hydrol Earth Syst Sci 2011;15(8):2747–61, http://dx.doi.org/10.5194/hess-15-2747-2011.

[15] Poretti I, Amicis M. An approach for flood hazard modelling and mapping in medium Valtellina. Nat Hazards Earth Syst Sci 2011;11:1141–51.

[16] Moya Quiroga V, Popescu I, Solomatine D, Bociort L. Cloud and cluster computing in uncertainty analysis of integrated flood models. J Hydroinf 2013;15:55–69.

[17] Knebl MR, Yang ZL, Hutchison K, Maidment DR. Regional scale flood modeling using NEXRAD rainfall, GIS, and HEC-HMS/RAS: a case study for the San Antonio River Basin Summer 2002 storm event. J Environ Manag 2005;75(4 special issue):325–36, http://dx.doi.org/10.1016/j.jenvman.2004.11.024.

[18] Lian JJ, Xu K, Ma C. Joint impact of rainfall and tidal level on flood risk in a coastal city with a complex river network: a case study of Fuzhou City, China. Hydrol Earth Syst Sci 2013;17(2):679–89, http://dx.doi.org/10.5194/hess-17-679-2013.

[19] Mohammadi SA, Nazariha M, Mehrdadi N. Flood damage estimate (quantity), using HEC-FDA model. Case study: the Neka river. Procedia Eng 2014;70:1173–82, http://dx.doi.org/10.1016/j.proeng.2014.02.130.

[20] Brunner G. Combined 1D and 2D modelling with HEC-RAS. USACE; 2014. p. 130.

[21] UNDP. Tras las huellas del cambio climático en Bolivia: Estado del arte del conocimiento sobre adaptación al cambio climatico—Agua y seguridad alimentaria [On the trail of climate change in Bolivia: state of the art of knowledge on adaptation to climate change—water and food security]. Programa de las Naciones Unidas para el Desarrollo Tech. Rep.; 2011. p. 144.

[22] Plotzki A, Jan-Hendrik M, Heinz V. Review of past and recent fluvial dynamics in the Beni lowlands, NE Bolivia. Geogr Helv 2011;66:164–72.

[23] Van Damme PA, Carvajal-Vallejos FM, Pouilly M, Perez T, Molina Carpio J. Amenazas para los peces y pesquerias de la Amazonia boliviana. In: Van Damme PA, Carvajal-Vallejos FM, Molina J, editors. Los Peces y Delfines de la Amazonia Boliviana: Habitats, Potencialidades y Amenazas. Cochabamba, Bolivia: INIA editorial; 2011. p. 327–65.

[24] Flood Observatory. The flood observatory; 2015. http://floodobservatory.colorado.edu. Last access January 2015.

[25] Vauchel P. Estudio de la crecida 2014 en la Cuenca del rio Madera. ORE HYBAM; 2014. p. 26.

[26] Espinoza JC, Marengo JA, Ronchail J, Molina J, Noriega L, Guyot JL. The extreme 2014 flood in South-Western Amazon basin: the role of tropical–subtropical south Atlantic SST gradient. Environ Res Lett 2014;9:1–9.

[27] Earth observatory NASA, 2014, Flooding in Bolivia: image of the day (online). http://earthobservatory.nasa.gov/IOTD/view.php?id=83337. Last access March 2015.

[28] SEMENA Servicio de mejoramiento de la navegacion Amazonica, http://www.semena.gob.bo. Last Access July 2015.

[29] Chow VT, Maidment DR, Mays LW. Hidrologia Aplicada. Santa Fe de Bogota, Colombia: McGrawHill; 1994. p. 584 [in Spanish].

[30] Moya Quiroga V, Kure S, Udo K, Mano A. Automating HEC-RAS input data and execution for improved hydraulic analysis: the Bolivian Amazonia 2014 flood. In: E-proceedings of the 36th IAHR world congress, 28 June - 03 July,. 2015. p. 1–9.

[31] Horrit M, Di Baldasarre G, Bates P, Brath A. Comparing the performance of a 2-D finite element and a 2-D finite volume model of floodplain inundation using airborne SAR imagery. Hydrol Process 2007;21:2745–59.

[32] Di Baldasarre G, Schumann G, Bates P. A technique for the calibration of hydraulic models using uncertain satellite observations of flood extent. J Hydrol 2009;367:276–82.

[33] MLIT. Flood hazard mapping manual in Japan. Ministry of Land Infrastructure and Transportation; 2005. p. 87.

[34] Horrit M, Bates P. Evaluation of 1D and 2D numerical models for predicting river flood inundation. J Hydrol 2002;268:87–99.

[35] MOD16. MODIS global evapotranspiration; 2015. http://www.ntsg.umt.edu/project/mod16. Last access July 2015.

[36] Balcazar HE. Problematica de las inundaciones en el Beni, Sociedad de Ingenieros de Bolivia, Marzo 2014. https://dl.dropboxusercontent.com/u/74077502/BENI/PROBLEM%C3%81TICA%20DE%20LAS%20INUNDACIONES%20EN%20EL%20BENI-2014-HEBR.pdf. Last access November 2015.

[37] Reliefweb; 2015. Beni: inundaciones cubren las carreteras en San Javier y aíslan a esa población con Trinidad, http://reliefweb.int/report/bolivia-plurinational-state/beni-inundaciones-cubren-las-carreteras-en-san-javier-y-slan-esa. Last access November 2015.

[38] Pongsumpum P. Mathematical model of Dengue disease with the incubation period of virus. World Acad Sci Eng Technol 2008;44:328–32.

[39] Verdonschot PFM, Besse-lototskaya AA. Limnologica Flight distance of mosquitoes (Culicidae): a metadata analysis to support the management of barrier zones around rewetted and newly constructed wetlands. Limnologica 2014;45:69–79, http://dx.doi.org/10.1016/j.limno.2013.11.002.

[40] Sistema de las Naciones Unidas y la Cruz Roja Boliviana. Bolivia: Emergencia inundaciones 2014, Reporte de situación, 20140311-SNU-BOL-SitRepNo_5, 2014. p. 8.

[41] Alvez N, da Costa Silva W, Leite J, Monteiro J, Lounibos L, Lourenco de Oliveira R. Dispersal of Aedes aegypti and Aedes albopictus (Diptera: Culicidae) in an Urban Endemic Dengue Area in the State of Rio de Janeiro, Brazil. Mem Inst Oswaldo Cruz 2003;98:191–8.